Kovove Mater. 58 2020 433–443
DOI: 10.4149/km_2020_6_433

The effect of heat treatment on microstructure and hardness of in-situ Ti-38Al-7.5Nb-5C-0.9Mo composite

A. Klimová*, J. Lapin

Institute of Materials and Machine Mechanics, Slovak Academy of Sciences, Dúbravská cesta 9, 845 13 Bratislava 3, Slovak Republic

Received 25 August 2020, received in revised form 15 September 2020, accepted 2 October 2020

Abstract

The effect of the solution annealing temperature and cooling rate on the microstructure and hardness of as-cast in-situ composite with nominal composition Ti-38Al-7.5Nb-5C-0.9Mo (at.%) was studied. The composite was prepared by vacuum induction melting in a graphite crucible, followed by centrifugal casting into the graphite mould. Heat treatment of the composite consisted of the solution annealing at 1200, 1300, and 1400 °C, followed by cooling to room temperature at two different cooling rates. The matrix of the as-cast composite consisting of α_2(Ti_3Al) and β/B2(Ti) phases is reinforced by uniformly distributed plate-like $(Ti,Nb)_2AlC$ and irregularly shaped particles composed of $(Ti,Nb)_2AlC$ and a small amount of (Ti,Nb)C phases. The applied heat treatment has no measurable effect on the volume fraction of the primary carbide particles. The solution annealing at 1300 and 1400 °C leads to the full transformation of the (Ti,Nb)C phase retained in the cores of irregularly shaped particles to the $(Ti,Nb)_2AlC$ phase. The cooling from thermodynamically stable $\beta + \alpha + (Ti,Nb)_2AlC$ phase-field at a rate of 5 °C min^{-1} results in the formation of lamellar $\alpha_2 + \gamma$ colonies with β/B2 and γ(TiAl) phases on their boundaries. The cooling from thermodynamically stable $\beta+\alpha+\gamma + (Ti,Nb)_2AlC$ phase-field results in the formation of a multi-phase matrix consisting of α_2, β/B2, and γ phases in the form of single-phase regions and a small amount of coarse lamellar $\alpha_2+\gamma$ regions. The increasing volume fraction of the β/B2 phase with the increasing solution annealing temperature leads to an increase in Vickers hardness of the composite.

K e y w o r d s: intermetallics, TiAl, composites, casting, microstructure, hardness

1. Introduction

Intermetallic TiAl based alloys are important light-weight materials for specific high-temperature structural applications in aerospace and automotive industries [1, 2]. Among various designed systems, β-solidifying TiAl based alloys show balanced mechanical properties when subjected to appropriate heat treatments [3, 4]. Additions of the strong β (Ti-based solid solution with a body-centred cubic crystal structure) stabilising elements such as Nb and Mo to TiAl based alloys contribute to the improvement of the creep, oxidation resistance, and room temperature ductility [2, 5]. The addition of carbon below 1 at.% results in their solid solution strengthening and precipitation strengthening by fine Ti_3AlC and Ti_2AlC carbide particles [6–9]. The increase of carbon content above 1 at.% leads to the in-situ formation of coarse primary Ti_2AlC particles during solidification, which offers an additional possibility to widen the processing window to optimise microstructural and mechanical properties for specific structural applications [10–16]. The thermo-chemically stable reinforcing Ti_2AlC particles are characterised by a high fracture resistance, good damage tolerance, high thermal conductivity, and density and thermal expansion coefficients similar to TiAl alloys [17]. Several methods based on ingot or powder metallurgy have been already applied successfully to fabricate in-situ metal matrix composites reinforced with carbide particles [18–20].

Several studies have been published on the effect of Al, Nb, and C content on the microstructure of

*Corresponding author: tel.: +421 2 3240 1055; e-mail address: alena.klimova@savba.sk

Table 1. Heat treatment of the composite

Heat treatment	Heating	Cooling
HT1-X	to a temperature of X at a heating rate of 10 °C min^{-1} holding for 1 h (X = 1200, 1300, 1400 °C)	water cooling to room temperature
HT2-X		cooling at a rate of 5 °C min^{-1} to a temperature of 700 °C followed by furnace cooling to room temperature
HT	to a temperature of 1420 °C at a heating rate of 10 °C min^{-1} holding for 10 min	furnace cooling to room temperature

the in-situ Ti-Al-Nb-Mo based composites prepared by the vacuum induction melting and solidification in graphite crucibles [21, 22] or by the casting to the graphite moulds [13, 15, 18, 23, 24]. In the studied in-situ composites, the content of Al, Nb, and C varied in the range from 37 to 47 at.%, from 3.5 to 8 at.%, and from 1 to 7 at.%, respectively. The addition of carbon from 1 to 7 at.% leads to the formation of the primary $(Ti,Nb)_2AlC$ particles during solidification. The carbon content affects both the morphology and volume fraction of primary $(Ti,Nb)_2AlC$ particles. As shown by Lapin et al. [13], while the content of carbon below 2 at.% leads to the formation of plate-like $(Ti,Nb)_2AlC$ particles, both plate-like and coarse irregularly shaped carbides are formed in the microstructure of the composites with the carbon content above 2 at.%. Residual (Ti,Nb)C phase with a significantly higher hardness and elastic modulus than those of $(Ti,Nb)_2AlC$ phase remains in some coarse irregularly shaped primary carbide particles of as-cast in-situ composites with Al content ranging from 37 to 47 at.% [18, 21, 23–25]. As shown by Lapin et al. [13, 26], hot isostatic pressing (HIP) at a temperature of 1250 °C for 4 h applied for removing casting porosity does not lead to a full transformation of the residual (Ti,Nb)C phase to $(Ti,Nb)_2AlC$. Hence, it is of large interest to extend the existing knowledge in this field about the solid-state phase transformations and elucidate the effect of solution annealing temperature not only on the microstructure of the intermetallic matrix but also on the evolution of chemical and phase composition of primary carbide particles in as-cast in-situ composites.

The present study aims to elucidate the effect of the solution annealing temperature and cooling rate on the microstructure and hardness of as-cast in-situ composite with nominal composition Ti-38Al-7.5Nb-5C-0.9Mo (at.%). The emphasis is given to solid-state phase transformations affecting the microstructure of the intermetallic matrix and also to the effect of solution annealing temperature on the stability of the residual (Ti,Nb)C phase in reinforcing carbide particles.

2. Experimental material and procedures

The composite with nominal composition Ti-38Al-7.5Nb-5C-0.9Mo (at.%) was prepared by vacuum induction melting of master alloy in graphite crucibles with an inner diameter of 45 mm and length of 75 mm. The vacuum chamber of the induction melting furnace was evacuated to a vacuum pressure of 4.5 Pa and flushed with argon three times. After increasing the vacuum pressure to 10^3 Pa by a partial filling with argon (purity of 99.9995 %), the charge was heated to a melt temperature of 1650 °C and held at this temperature for 30 s. The temperature of the melt was measured by a pyrometer. The melt was centrifugally cast into a cold graphite mould at a rotation speed of 250 rpm under a vacuum pressure of 10^3 Pa. The centrifugally cast conical samples with a minimum diameter of 12 mm, a maximum diameter of 14 mm, and a length of 150 mm were removed from the mould and cut to smaller pieces with a length of 20 mm for heat treatments and metallographic observations.

The samples of the composite were subjected to the heat treatment under argon atmosphere consisting of heating to a solution annealing temperature of 1200, 1300, and 1400 °C at a heating rate of 10 °C min^{-1}, holding at this temperature for 1 h and subsequent cooling to the room temperature with two different cooling rates, as is described in Table 1 (HT1-X and HT2-X). The temperature of the samples was continuously monitored by Pt-PtRh10 thermocouple, touching the sample surface during solution annealing. The acquisition of time-temperature data was performed electronically using an acquisition modulus and computer.

For the determination of the solid-state phase transformation temperatures, the differential thermal analysis (DTA) was performed in alumina crucibles using alumina powder as the reference standard. The samples for DTA experiments with a diameter of 6 mm and length of 7 mm were cut from the composite annealed at a temperature of 1420 °C for 10 min and furnace cooled to room temperature (HT in Table 1). The DTA samples were heated to a temperature of 1450 °C

at a heating rate of 10 °C min^{-1}, held at this temperature for 10 min, and then cooled to room temperature at a cooling rate of 10 °C min^{-1} under protective argon atmosphere.

Standard metallographic techniques such as grinding on SiC papers, polishing on diamond paste with various grain sizes ranging from 10 to 0.25 μm, and etching in a solution of 100 ml H_2O, 6 ml HNO_3, and 3 ml HF were used. Microstructure investigations were performed by scanning electron microscopy (SEM), scanning electron microscopy in backscattered electron (BSE) mode, and X-ray diffraction analysis (XRD). XRD analysis was carried out by a diffractometer equipped with an X-ray tube with a rotating Cu anode operating at 12 kW. Chemical composition of the in-situ composites was analysed by energy-dispersive spectrometry (EDS) calibrated using the standards for measurements of the composition of carbides (TiC, Ti_2AlC). The average content of carbon in the samples was measured by LECO CS844 elemental analyser. Size, morphology, and volume fraction of the coexisting phases were determined from the digitalised micrographs using a computer image analyser, and measured data were treated by statistical methods.

Vickers hardness measurements were performed by a universal hardness testing machine at an applied load of 298 N, holding time at the point of load application of 2 s and rate of load application of 15 N s^{-1} on the as-cast and heat-treated samples. Instrumented nanoindentation measurements of coexisting phases were carried out at an applied load of 0.005 N and holding time at the point of load application of 2 s on polished and slightly etched samples using a nanoindenter with Berkovich tip of the indenter. The indentation nanohardness and elastic modulus of the coexisting phases in the as-cast and heat-treated composite were determined from the statistical evaluation of 100 random indentations in each phase.

3. Results

3.1. Microstructure characterisation

3.1.1. As-cast composite

The average chemical composition of the as-cast composite was measured using both the EDS method combined with the analysis of carbon using LECO

Table 2. The average chemical composition of as-cast composite and coexisting phases measured by EDS and LECO CS844 elemental analyser

Sample	Region	Phase composition	Element (at.%)				
			Ti	Al	Nb	Mo	C
as-cast	1	$(Ti,Nb)_2AlC$	44.7 ± 0.4	24.2 ± 0.4	5.1 ± 0.9	–	26.0 ± 0.8
	2	(Ti,Nb)C	44.5 ± 3.0	2.1 ± 2.0	4.5 ± 0.4	–	48.9 ± 1.7
	3	β/B2	50.8 ± 0.5	38.8 ± 0.5	9.0 ± 0.1	1.4 ± 0.1	–
	4	α_2	49.0 ± 0.5	42.5 ± 0.7	7.6 ± 0.7	0.9 ± 0.1	–
Composite			48.6 ± 0.2	37.9 ± 0.4	7.6 ± 0.1	0.9 ± 0.1	5.0 ± 0.1

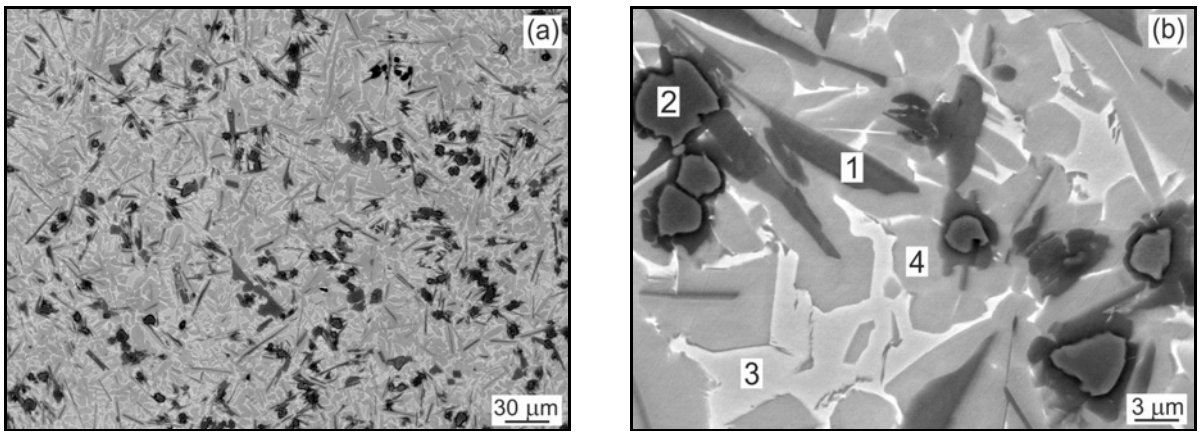

Fig. 1. (a) The typical microstructure of the as-cast composite, BSE. (b) Primary plate-like and irregularly shaped carbide particles in the two-phase matrix, BSE. The measured chemical composition of phases marked in the figure is summarised in Table 2.

Table 3. Volume fraction V_p, length of major axis L_{maj}, length of minor axis L_{min}, and aspect ratio A_R of the primary plate-like and irregularly shaped carbide particles in the as-cast composite

Morphology of particles	V_p (vol.%)	L_{maj} (μm)	L_{min} (μm)	A_R
Plate-like	1.9 ± 0.5	4.84 ± 0.18	0.42 ± 0.01	14.54 ± 0.42
Irregularly shaped	13.7 ± 1.0	10.37 ± 0.27	3.65 ± 0.14	3.23 ± 0.06

Table 4. Volume fraction of $(Ti,Nb)_2AlC$, (Ti,Nb)C, α_2, γ, and β/B2 phase regions in the as-cast composite

As-cast sample	Phase				
	(Ti,Nb)C	$(Ti,Nb)_2AlC$	α_2	β/B2	γ
V (vol.%)	2.9 ± 0.5	12.7 ± 1.0	59.3 ± 1.6	24.4 ± 0.8	0.7 ± 0.5

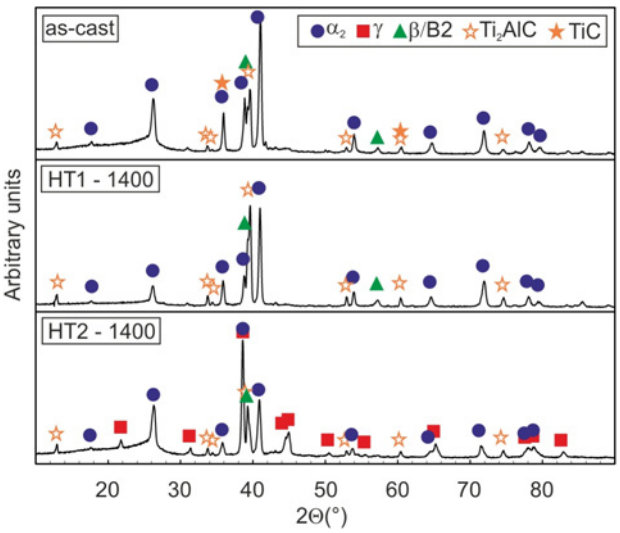

Fig. 2. XRD patterns of the as-cast and heat-treated composite. The identified coexisting phases are indicated in the figure.

CS844 elemental analyser (Table 2). Figure 1 shows the typical microstructure of the as-cast composite. The microstructure consists of the primary carbide particles relatively uniformly distributed in the matrix, as seen in Fig. 1a. The volume fraction of the carbide particles is measured to be (15.6 ± 1.0) vol.%. Two morphologies of the primary carbides can be distinguished in the microstructure of the as-cast composite: irregularly shaped (85 %) and plate-like (15 %) particles, as shown in Table 3. The coexisting phases in the composite are identified on the base of the microstructure observations (Fig. 1b), XRD analyses (Fig. 2), and measurements of the chemical composition of the particles and coexisting microstructural regions (Table 2). The carbide particles are composed of $(Ti,Nb)_2AlC$ (region 1), and residual (Ti,Nb)C phase (region 2) observed in the cores of some irregularly shaped carbide particles, as shown in Fig. 1b. The (Ti,Nb)C phase represents about 20 % of the volume fraction of the primary carbide particles in the as-cast composite, as seen in Table 4. The matrix of the composite consists of $\alpha_2(Ti_3Al)$ and β/B2 (ordered body-centred cubic crystal structure) phase, as seen in Fig. 1b. The volume fraction of the α_2 phase reaches nearly 60 vol.%, which is a significantly higher value than that of the β/B2 phase (Table 4). As has been already discussed in detail in the recent work on the microstructure formation in the composites with a similar chemical composition [18], the fast cooling rates significantly suppress the nucleation and growth of γ(TiAl) lamellae in the α/α_2 phase during the centrifugal casting.

Table 2 indicates that the solubility of Nb in (Ti,Nb)C and $(Ti,Nb)_2AlC$ is high and reaches up to 60–70 % of the average content of Nb in the composite. On the other hand, Mo content is under detectable limits of the applied EDS analysis in all primary carbide particles, including their cores. During solidification, Nb and Mo segregate preferentially to dendrites, and their content in the remaining β/B2 phase exceeds their average content in the composite (Table 2).

3.1.2. Heat treatment HT1-X

The water quenching was applied to preserve the microstructures of the studied in-situ composite at three different solution annealing temperatures of 1200, 1300, and 1400 °C. The effect of the heat treatment HT1-X on the phase composition and microstructure of the composite is shown in Figs. 2 and 3. The microstructure of the composite subjected to the heat treatment HT1-1200 consists of the matrix containing α_2, β/B2, and γ phases mainly in the form of single-phase regions, a small amount of coarse lamellar $\alpha_2 + \gamma$ regions, plate-like $(Ti,Nb)_2AlC$ particles, and coarse irregularly shaped carbides composed of $(Ti,Nb)_2AlC$ and (Ti,Nb)C phases, as shown in

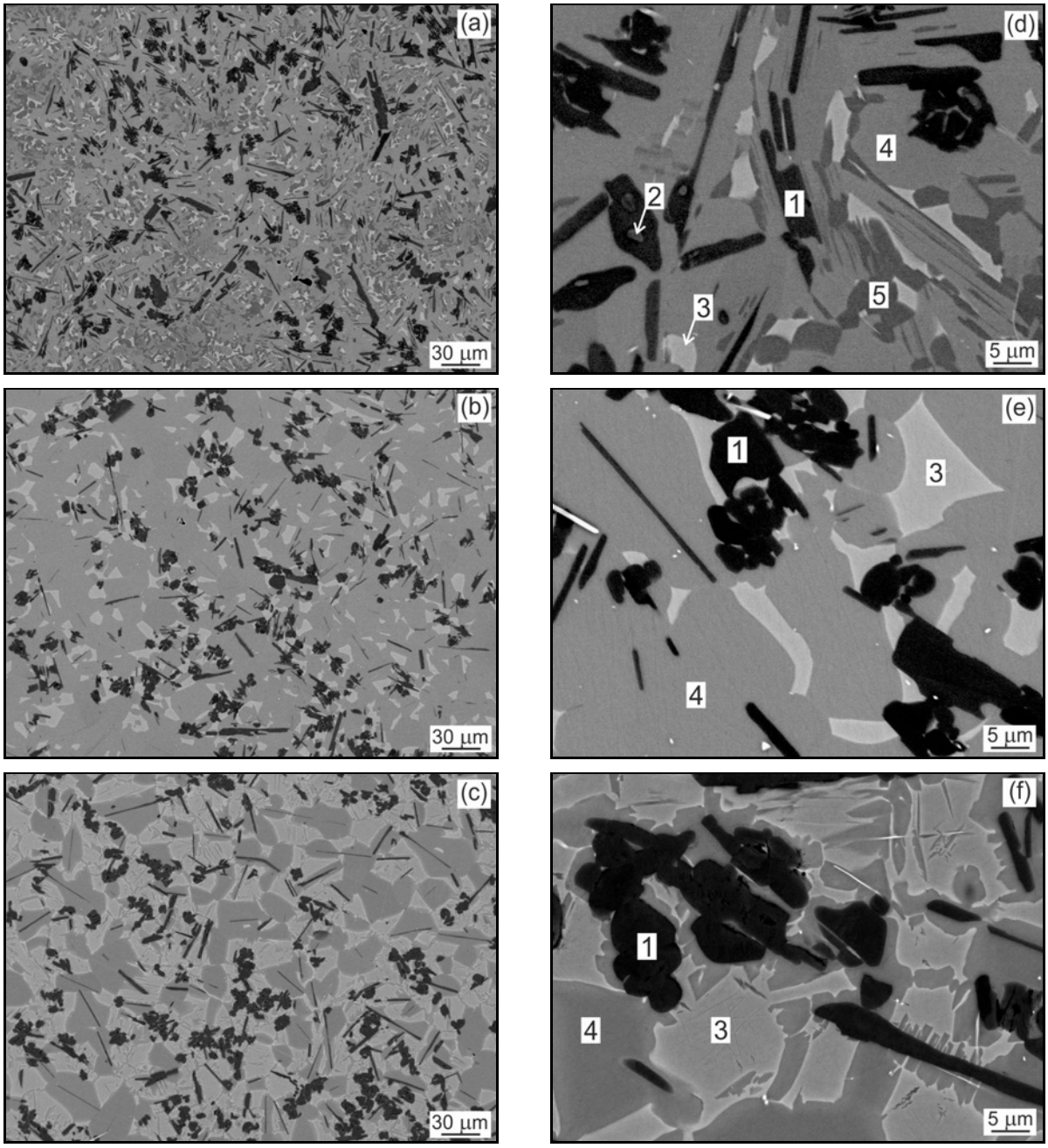

Fig. 3. The microstructure of the composite after the heat treatment HT1-X, BSE: (a), (d) HT1-1200; (b), (e) HT1-1300; and (c), (f) HT1-1400. The chemical compositions of phases marked in the figures are summarised in Table 5.

Figs. 3a and 3d. The heat treatment HT1-1300 leads to the formation of single-phase $(Ti,Nb)_2AlC$ particles at the expense of full dissolution of the retained (Ti,Nb)C phase and the matrix composed of α_2 and β/B2 phases, as seen in Figs. 3b and 3e. The heat treatment HT1-1400 affects the morphology and distribution of the coexisting α_2 and β/B2 phases in the matrix but has no significant effect on the reinforcing single-phase $(Ti,Nb)_2AlC$ particles compared to those in the composite subjected to the heat treatment HT1--1300, as seen in Figs. 3c and 3f.

Figure 4a shows the effect of the applied heat treatment HT1-X on the volume fraction of carbide particles and coexisting phases in the matrix. The solution annealing temperature has no measurable effect on the volume fraction of the primary carbide particles, and all differences fall into experimental errors of the measurements. On the other hand, the volume fractions of the coexisting phases in the matrix are significantly affected by the solution annealing temperature. The volume fraction of the β/B2 phase increases with the increasing solution annealing temperature. The vol-

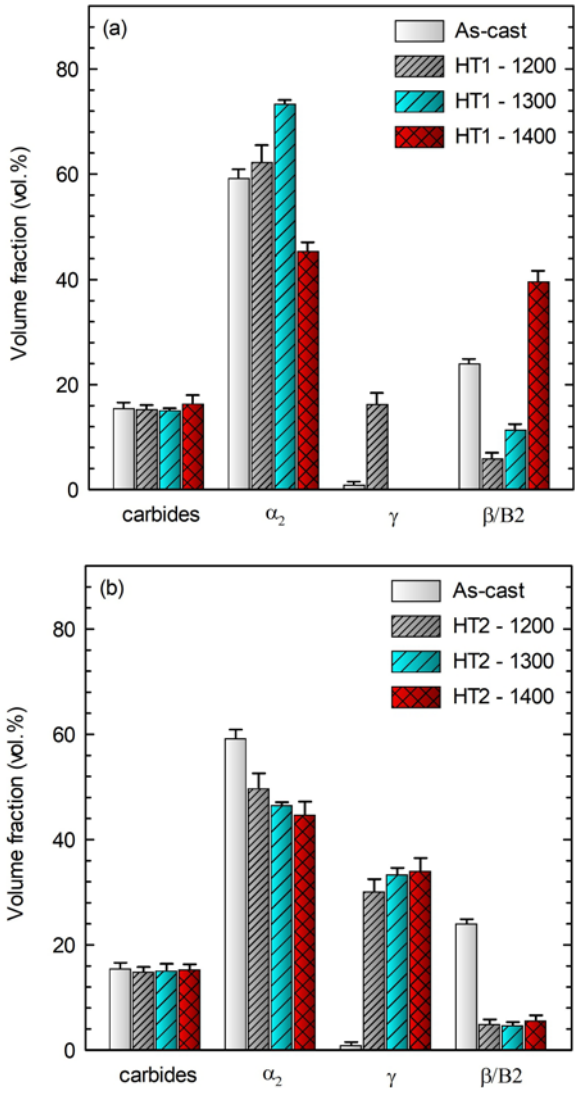

Fig. 4. The volume fraction of primary carbides and coexisting α_2, γ, and β/B2 phases in the heat-treated composite: (a) HT1-X, (b) HT2-X.

ume fraction of α_2 reaches a maximum value after the heat treatment HT1-1300 and is decreased at the expense of the formation of γ and β/B2 phase in the samples subjected to the heat treatments HT1-1200 and HT1-1400, respectively.

Table 5 shows the effect of the applied heat treatments HT1-1200, HT1-1300, and HT1-1400 on the chemical composition of coexisting phases in the composite. The content of Nb and Mo in the β/B2 phase is higher than the average content of these elements in the composite and increases with the decreasing volume fraction of the β/B2 phase. The solution annealing temperature has no significant effect on the content of Nb and Mo in the α_2 phase. The Al content in the α_2 and β/B2 phases does not change significantly after the heat treatments HT1-1300 and HT1-1400 in comparison with the as-cast state, but the formation of the γ phase in the microstructure leads to the decrease of Al content in both α_2 and β/B2 phases during the heat treatment HT1-1200.

3.1.3. Heat treatment HT2-X

Figure 5 shows the effect of heat treatment HT2-X on the microstructure of the studied composite. The heat treatment HT2-1200 leads to the formation of the matrix composed of α_2, β/B2, γ, and lamellar $\alpha_2+\gamma$ regions, as seen in Figs. 5a and 5d. The residual (Ti,Nb)C phase remains in the cores of some coarse irregularly shaped $(Ti,Nb)_2AlC$ particles (Fig. 5d). Despite different solution annealing temperature, the heat treatments HT2-1300 and HT2-1400 result in the formation of very similar microstructures of the composite, as shown in Figs. 5b and 5c. The reinforcing $(Ti,Nb)_2AlC$ particles are surrounded by the matrix consisting of the lamellar $\alpha_2+\gamma$, β/B2, and γ regions, as shown in Figs. 5e and 5f. While the coarse irregularly shaped $(Ti,Nb)_2AlC$ particles are distributed preferentially within the γ phase formed along the lamellar grain boundaries, the plate-like particles are found in both lamellar grains and within the γ phase formed along the lamellar grain boundaries. Occasionally, the β/B2 phase is preserved in the clustered $(Ti,Nb)_2AlC$ particles, as seen in Figs. 5d–f.

Figure 4b shows the effect of the heat treatment HT2-X on the volume fraction of carbide particles and coexisting phases in the matrix. The volume fraction of the α_2 phase decreases. The volume fraction of the γ phase increases with the increasing solution annealing temperature compared to that in the as-cast and heat-treated HT1-X samples. On the other hand, the solution annealing temperature has no measurable effect on the volume fraction of the primary carbide particles. All differences fall into experimental errors of the measurements.

Table 5 indicates that the heat treatment HT2-X carried out at a cooling rate of $5\,℃\,min^{-1}$ leads to an increase of the content of Nb and Mo in β/B2 phase compared to that in the samples subjected to the heat treatment HT1-X, which can be attributed to significantly different cooling rates applied during these two heat treatments.

3.2. Hardness and nanohardness

Figure 6 shows measured hardness and nanohardness of coexisting phases of the as-cast, HT1-X, and HT2-X samples. Figure 6a shows Vickers hardness HV30 of the as-cast and heat-treated samples. The results of the measurement of indentation nanohardness H_{IT} in the (Ti,Nb)C, $(Ti,Nb)_2AlC$, β/B2, α_2, and γ phases of the as-cast and heat-treated composite are shown in Fig. 6b. Since the solution annealing tempe-

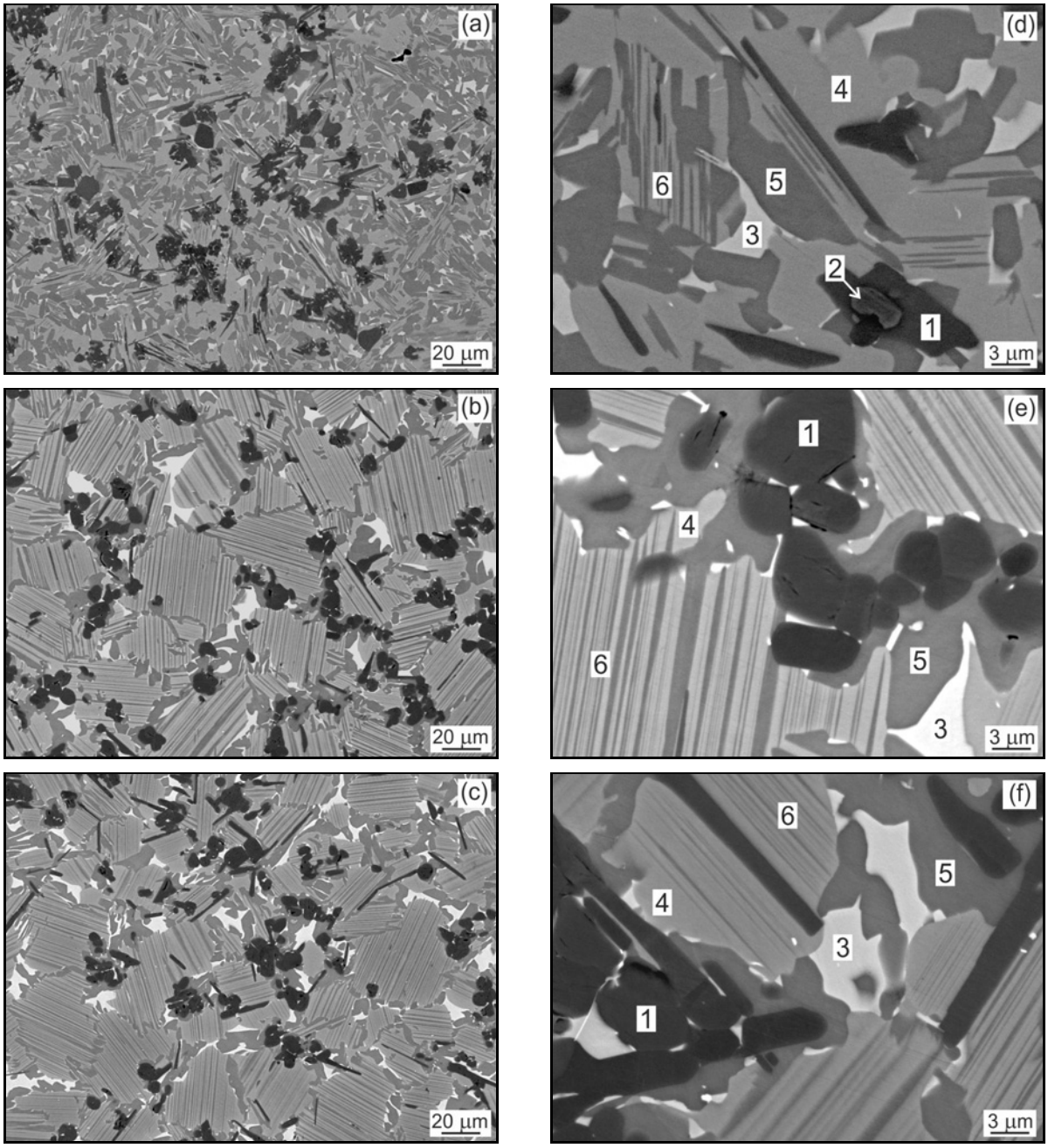

Fig. 5. The microstructure of the composite after the heat treatment HT2-X, BSE: (a), (d) HT2-1200; (b), (e) HT2-1300; and (c), (f) HT2-1400. The chemical composition of phases and regions marked in the figures are summarised in Table 5.

rature ranging from 1200 to 1400 ℃ has no measurable effect on indentation nanohardness of the coexisting phases and all differences fall into experimental errors of the measurements, the measured average values of H_{IT} for the heat-treated samples are plotted only as HT1 and HT2 without specification of solution annealing temperature.

The measured nanohardness of (Ti,Nb)C of 38 GPa exceeds more than twice the nanohardness of $(Ti,Nb)_2AlC$ phase, and this value falls within the wide range of 25–50 GPa reported by Hua et al. [27] for TiC particles in intermetallic Ni_3Al matrix. The elastic modulus of $(Ti,Nb)_2AlC$ phase is measured to be 238 GPa, which corresponds to the values of 220–240 GPa published by Wei at al. [25] for Ti_2AlC particles in TiAl-based matrix composite. The elastic modulus of (Ti,Nb)C is measured to be 408 GPa and falls within a range of the calculated and measured values of 310–450 GPa published for TiC [28, 29]. Both the hardness and elastic modulus of the TiC phase depend on its stoichiometry and porosity. The measured elastic modulus of (Ti,Nb)C in the studied compos-

Table 5. The chemical composition of the coexisting phases and microstructural regions in the heat-treated composite measured by EDS

Sample		Region	Phase composition	Element (at.%)				
			Ti	Al	Nb	Mo	C	
HT1	1200	1	$(Ti,Nb)_2AlC$	43.9 ± 2.4	24.3 ± 0.5	5.5 ± 0.4	–	26.3 ± 1.3
		2	(Ti,Nb)C	46.1 ± 2.5	1.4 ± 1.0	4.4 ± 0.5	–	47.1 ± 1.6
		3	β/B2	51.4 ± 0.7	36.9 ± 0.9	9.1 ± 0.2	2.6 ± 0.3	–
		4	α_2	52.4 ± 0.2	38.9 ± 0.2	7.8 ± 0.1	1.0 ± 0.1	–
		5	γ	46.9 ± 0.3	44.4 ± 0.2	7.9 ± 0.1	0.8 ± 0.1	–
	1300	1	$(Ti,Nb)_2AlC$	44.6 ± 1.5	24.4 ± 0.1	5.3 ± 0.3	–	25.7 ± 1.3
		3	β/B2	50.2 ± 0.2	39.0 ± 0.5	9.0 ± 0.1	1.9 ± 0.1	–
		4	α_2	50.2 ± 0.2	41.0 ± 0.2	7.8 ± 0.1	1.0 ± 0.1	–
	1400	1	$(Ti,Nb)_2AlC$	44.9 ± 0.4	24.8 ± 0.4	5.2 ± 0.9	–	25.1 ± 1.0
		3	β/B2	49.9 ± 0.3	40.0 ± 0.6	8.7 ± 0.1	1.4 ± 0.1	–
		4	α_2	49.2 ± 0.4	42.4 ± 0.6	7.7 ± 0.7	0.7 ± 0.1	–
HT2	1200	1	$(Ti,Nb)_2AlC$	44.0 ± 1.0	24.4 ± 0.6	5.4 ± 0.4	–	26.2 ± 0.9
		2	(Ti,Nb)C	45.3 ± 1.9	1.7 ± 1.2	4.5 ± 0.7	–	48.5 ± 1.5
		3	β/B2	51.1 ± 0.6	35.7 ± 0.8	9.3 ± 0.4	4.0 ± 0.8	–
		4	α_2	53.5 ± 0.8	37.5 ± 0.6	8.0 ± 0.1	1.0 ± 0.1	–
		5	γ	46.2 ± 0.3	45.2 ± 0.3	7.9 ± 0.1	0.7 ± 0.1	–
	1300	1	$(Ti,Nb)_2AlC$	44.4 ± 0.8	24.1 ± 0.5	5.4 ± 0.5	–	26.1 ± 0.8
		3	β/B2	52.0 ± 0.9	35.0 ± 1.0	9.5 ± 0.6	3.6 ± 1.0	–
		4	α_2	51.8 ± 0.3	39.0 ± 0.2	8.2 ± 0.1	1.0 ± 0.1	–
		5	γ	45.7 ± 0.2	45.3 ± 0.5	8.3 ± 0.2	0.7 ± 0.1	–
		6	$\alpha_2 + \gamma$	50.3 ± 0.8	40.3 ± 1.0	8.4 ± 0.5	1.0 ± 0.3	–
	1400	1	$(Ti,Nb)_2AlC$	44.8 ± 0.4	24.4 ± 0.2	5.2 ± 0.1	–	25.6 ± 0.6
		3	β/B2	51.6 ± 0.2	34.6 ± 0.2	9.9 ± 0.2	3.9 ± 0.2	–
		4	α_2	51.6 ± 1.0	39.3 ± 1.2	8.1 ± 0.2	0.9 ± 0.1	–
		5	γ	45.9 ± 0.6	45.2 ± 0.2	8.1 ± 0.4	0.8 ± 0.1	–
		6	$\alpha_2 + \gamma$	50.9 ± 0.9	40.5 ± 1.2	7.8 ± 0.2	0.8 ± 0.1	–

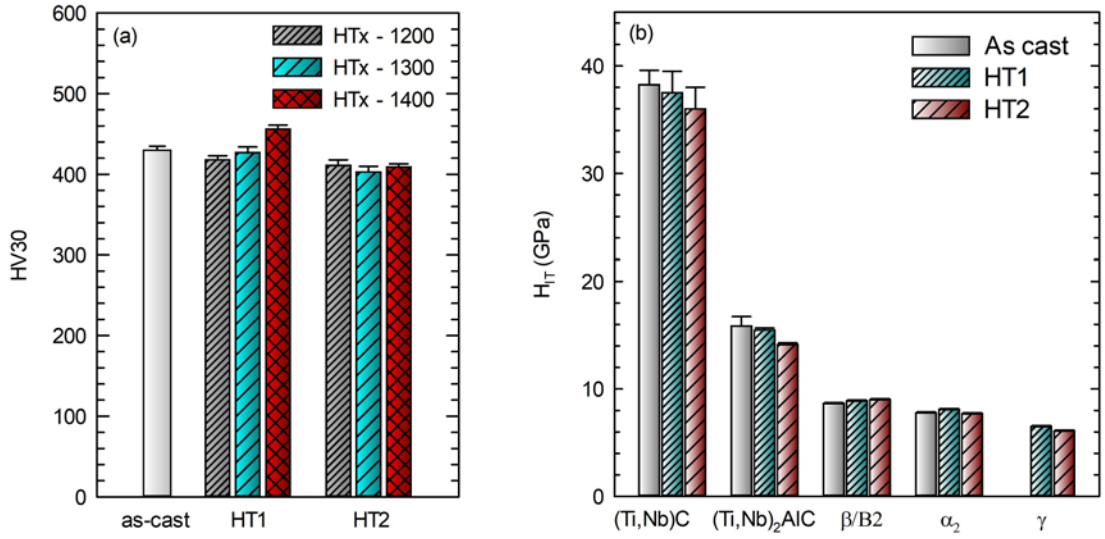

Fig. 6. (a) Vickers hardness HV30 of as-cast and heat-treated composite. (b) Indentation nanohardness H_{IT} of the (Ti,Nb)C, $(Ti,Nb)_2AlC$, β/B2, α_2, and γ phases. The nanohardness of (Ti,Nb)C is measured in the as-cast and heat-treated HT1-1200 composite. The nanohardness of γ phase is measured in the samples subjected to the heat treatments HT1-1200 and HT2-X.

ite is also affected by partial substitution of Ti by Nb atoms.

As shown in Fig. 6b, the nanohardness of (Ti,Nb)C and $(Ti,Nb)_2AlC$ phases is affected by the cooling rate during heat treatment. The nanohardness of the (Ti,Nb)C and $(Ti,Nb)_2AlC$ phases decreases with decreasing cooling rate. Still, the cooling rate has no statistically significant effect on the nanohardness of coexisting phases in the matrix, as shown in Fig. 6b.

4. Discussion

4.1. Formation of the microstructure

As shown by Witusiewicz et al. [30], the formation of Ti_2AlC particles in the ternary Al-C-Ti system follows the phase transformation sequence L (liquid) + $TiC_{1-x} \rightarrow L + Ti_2AlC$. Lapin et al. [30] have reported that the alloying of TiAl based matrix in-situ composites with Nb leads to partial substitution of Ti by Nb in both TiC and Ti_2AlC phases. Hence, the observed residual (Ti,Nb)C phase observed in some coarse irregularly shaped $(Ti,Nb)_2AlC$ particles represents a thermodynamically unstable phase preserved due to the relatively high cooling rates during the centrifugal casting of the composite. As seen in Fig. 3c, the irregularly shaped carbide particles are surrounded predominantly by the β/B2 phase indicating that the β phase nucleates directly on the primary carbides during solidification. The thin plate-like $(Ti,Nb)_2AlC$ particles are observed mostly in the α_2 phase regions, which indicates that they are formed from the liquid supersaturated by carbon during the last stages of solidification. Figure 7b shows the DTA heating curve of the studied composite with the initial microstructure shown in Fig. 7a. During the heating stage, the γ phase starts to transform into the α phase at a temperature of 1220 °C, and the transformation is finished at a temperature of 1270 °C. The heating curve indicates no significant change in the volume fraction of the coexisting α and β phases between 1270 and 1310 °C. At temperatures higher than 1310 °C, the volume fraction of the β phase continuously increases with increasing temperature at the expense of decreasing volume fraction of the α phase. Figures 3 and 4 confirm a significant increase in the volume fraction of the β phase from 12 vol.% at 1300 °C to 40 vol.% at 1400 °C measured in the water quenched HT1-1300 and HT1-1400 samples.

The heat treatment consisting of the solution annealing at temperatures corresponding to the thermodynamically stable $\beta + \alpha + \gamma + (Ti,Nb)_2AlC$ phase-field followed by cooling at a rate 5 °C min^{-1} (HT2--1200) results in the formation of low volume fraction of lamellar regions with thick non-uniform $\alpha_2 + \gamma$ lamellae. The remaining α_2 phase forms irregularly

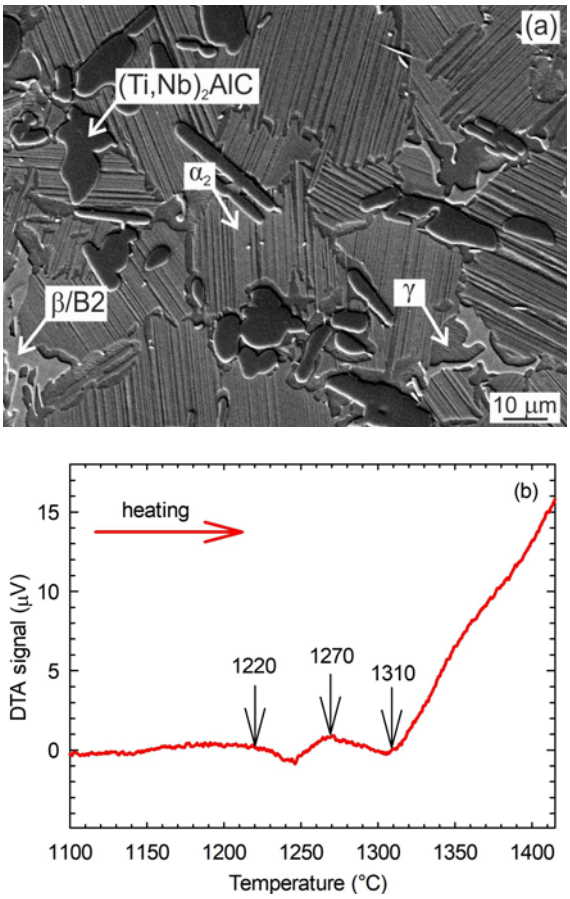

Fig. 7. (a) Initial microstructure of the DTA sample, SEM; (b) DTA heating curve of the studied composite.

shaped regions, as seen in Fig. 5a. The heat treatment consisting of the solution annealing at temperatures corresponding to the thermodynamically stable $\beta+\alpha + (Ti,Nb)_2AlC$ phase-field followed by cooling at a rate of 5 °C min^{-1} (HT2-1300 and HT2-1400) leads to the formation of 60 vol.% of lamellar $\alpha_2+\gamma$ colonies, as shown in Figs. 5b and 5c. Although different volume fractions of β and α phases are formed at the annealing temperatures of 1300 and 1400 °C, the volume fractions of coexisting regions in the heat-treated HT2--1300 and HT2-1400 samples are close to each other, indicating that a nearly thermodynamically equilibrium state is achieved due to low applied cooling rate. Higher cooling rates lead to differences in the volume fraction of coexisting regions between the samples annealed at 1300 and 1400 °C, which is confirmed by water quenching experiments applied for the heat-treated samples HT1-1300 and HT1-1400. The achieved results indicate that the microstructure and properties of the studied in-situ composite can be controlled by the selection of solution annealing temperature and the cooling rate, which affect significantly the formation of lamellar $\alpha_2 + \gamma$ structure and dissolution of the retained (Ti,Nb)C

phase in the coarse primary carbide particles [18, 31].

4.2. Hardness of the composite

During the solution annealing at 1300 and 1400 °C, the hard (Ti,Nb)C phase transforms fully to $(Ti,Nb)_2AlC$ phase, which leads to the softening of the reinforcing particles. As reported by Lapin et al. [13], the hardness of the TiAl based matrix composites reinforced by up to 20 vol.% of carbide particles is controlled by the hardness of the matrix and volume fraction of $(Ti,Nb)_2AlC$ particles. As shown in Fig. 6b, the highest nanohardness in the matrix is measured for the β/B2 phase, and the lowest for the γ phase. The increasing volume fraction of the β/B2 phase with the increasing solution annealing temperature (Fig. 4a) affects the hardness of the matrix. It results in the increasing hardness of the composite with increasing annealing temperature after the heat treatment HT1--X, as shown in Fig. 6a. The decrease of the volume fraction of the β/B2 phase to around 6 vol.% and increase of the volume fraction of the soft γ phase (Fig. 4b) lead to the softening of the composite after the heat treatment HT2-X compared with the as-cast state, as seen in Fig. 6a. Despite the variation in the morphology of the coexisting phases in the matrix of the composite, the measured hardness values vary only within the experimental errors of the measurements after the heat treatments HT2--1200, HT2-1300, and HT2-1400.

5. Conclusions

The effect of heat treatment on microstructure and hardness of as-cast in-situ composite with nominal composition Ti-38Al-7.5Nb-5C-0.9Mo (at.%) was studied. The following conclusions are reached:

1. The microstructure of the as-cast composite is formed by an intermetallic matrix reinforced by relatively uniformly distributed primary plate-like and irregularly shaped carbide particles. The matrix of the composite consists of α_2 and β/B2 phases. The primary carbide particles are composed of $(Ti,Nb)_2AlC$ phase and a small amount of (Ti,Nb)C phase preserved in the cores of some coarse irregularly shaped carbides.

2. The solution annealing at 1300 and 1400 °C followed by water quenching (HT1) or cooling at a rate of 5 °C min^{-1} (HT2) leads to the formation of single-phase $(Ti,Nb)_2AlC$ particles at the expense of full dissolution of the retained (Ti,Nb)C phase. After both heat treatments at the temperature of 1200 °C, (Ti,Nb)C phase remains in some coarse irregularly shaped carbides. The solution annealing temperature and the cooling rate have no measurable effect on the volume fraction of the primary carbide particles.

3. The heat treatments in thermodynamically stable $\beta + \alpha + \gamma + (Ti,Nb)_2AlC$ phase-field result in the formation of the multi-phase matrix, consisting of α_2, β/B2, and γ phases in the form of single-phase regions and a small amount of coarse lamellar $\alpha_2 + \gamma$ regions. Cooling at a rate of 5 °C min^{-1} leads to the higher volume fraction of the γ phase regions in the composite in comparison with the water quenched samples.

4. The heat treatments in thermodynamically stable $\beta + \alpha + (Ti,Nb)_2AlC$ phase-field result in the matrix of the composite consisting of α_2 and β/B2 phases in the water quenched samples. Cooling at a rate of 5 °C min^{-1} leads to the formation up to 60 vol.% of lamellar $\alpha_2 + \gamma$ colonies with β/B2 and γ phases on their boundaries.

5. The Vickers hardness of the composite depends on the microstructure of the matrix. The increasing volume fraction of the β/B2 phase leads to an increase in the hardness of the composite after the heat treatment consisting of the solution annealing followed by water quenching of the samples. The applied solution annealing temperatures have no significant effect on Vickers hardness of the samples prepared at a cooling rate of 5 °C min^{-1}.

Acknowledgements

This research was funded by the Slovak Research and Development Agency under the contract APVV-15-0660 and Slovak Grant Agency for Science under the contract VEGA 2/0074/19. The experimental work was carried out thanks to the infrastructure funded by the Research and Development Operational Program funded by the European Regional Development Fund under the contract ITMS 26240220081 in the frame of the project: Industrial Research Centre for operating lifetime of selected components of power plants.

References

[1] H. Clemens, S. Mayer, Intermetallic titanium aluminides in aerospace applications – processing, microstructure and properties, Mater. High Temp. 33 (2016) 560–570. doi:10.1080/09603409.2016.1163792

[2] F. Appel, H. Clemens, F. D. Fischer, Modeling concepts for intermetallic titanium aluminides, Prog. Mater. Sci. 81 (2016) 55–124. doi:10.1016/j.pmatsci.2016.01.001

[3] H. Clemens, S. Mayer, Design, processing, microstructure, properties, and applications of advanced intermetallic TiAl alloys, Adv. Eng. Mater. 15 (2013) 191–215. doi:10.1002/adem.201200231

[4] K. Kamyshnykova, J. Lapin, Grain refinement of cast peritectic TiAl-based alloy by solid-state phase transformations, Kovove Mater. 56 (2018) 277–287. doi:10.4149/km_2018_5_277

[5] H. Clemens, H. F. Chladil, W. Wallgram, G. A. Zickler, R. Gerling, K. D. Liss, S. Kremmer, V.

Guther, W. Smarsly, In and ex situ investigations of the β-phase in a Nb and Mo containing γ--TiAl based alloy, Intermetallics 16 (2008) 827–833. doi:10.1016/j.intermet.2008.03.008

[6] T. Klein, M. Schachermayer, F. Mendez-Martin, T. Schöberl, B. Rashkova, H. Clemens, S. Mayer, Carbon distribution in multi-phase γ-TiAl based alloys and its influence on mechanical properties and phase formation, Acta Mater. 94 (2015) 205–213. doi:10.1016/j.actamat.2015.04.055

[7] C. Scheu, E. Stergar, M. Schober, L. Cha, H. Clemens, A. Bartels, F. P. Schimansky, A. Cerezo, High carbon solubility in a γ-TiAl-based Ti-45Al-5Nb-0.5C alloy and its effect on hardening, Acta Mater. 57 (2009) 1504–1511. doi:10.1016/j.actamat.2008.11.037

[8] E. Schwaighofer, B. Rashkova, H. Clemens, A. Stark, S. Mayer, Effect of carbon addition on solidification behavior, phase evolution and creep properties of an intermetallic β-stabilized γ-TiAl based alloy, Intermetallics 46 (2014) 173–184. doi:10.1016/j.intermet.2013.11.011

[9] L. Wang, U. Lorenz, M. Münch, A. Stark, F. Pyczak, Influence of alloy composition and thermal history on carbide precipitation in γ-based TiAl alloys, Intermetallics 89 (2017) 32–39. doi:10.1016/j.intermet.2017.05.006

[10] R. Chen, H. Fang, X. Chen, Y. Su, H. Ding, J. Guo, H. Fu, Formation of TiC/Ti_2AlC and $\alpha_2+\gamma$ in in-situ TiAl composites with different solidification paths, Intermetallics 81 (2017) 9–15. doi:10.1016/j.intermet.2017.02.025

[11] H. Fang, R. Chen, Y. Yang, Y. Su, H. Ding, J. Guo, H. Fu, Role of graphite on microstructural evolution and mechanical properties of ternary TiAl alloy prepared by arc melting method, Mater. Des. 156 (2018) 300–310. doi:10.1016/j.matdes.2018.06.048

[12] Z. Wu, R. Hu, T. Zhang, F. Zhang, H. Kou, J. Li, Understanding the role of carbon atoms on microstructure and phase transformation of high Nb containing TiAl alloys, Mater. Charact. 124 (2017) 1–7. doi:10.1016/j.matchar.2016.12.008

[13] J. Lapin, A. Klimová, Z. Gabalcová, T. Pelachová, O. Bajana, M. Štamborská, Microstructure and mechanical properties of cast in-situ TiAl matrix composites reinforced with $(Ti,Nb)_2AlC$ particles, Mater. Des. 133 (2017) 404–415. doi:10.1016/j.matdes.2017.08.012

[14] M. Štamborská, J. Lapin, O. Bajana, Effect of carbon on room temperature compressive behaviour of Ti-44.5Al-8Nb-0.8Mo-xC alloys prepared by vacuum induction melting, Kovove Mater. 56 (2018) 349–356. doi:10.4149/km_2018_6_349

[15] J. Lapin, A. Klimová, M. Štamborská, K. Kamyshnykova, T. Pelachová, Development and properties of cast TiAl matrix in situ composites reinforced with carbide particles, Mater. Sci. Forum 941 (2018) 1907–1913. doi:10.4028/www.scientific.net/MSF.941.1907

[16] H. Fang, R. Chen, X. Gong, Y. Su, H. Ding, J. Guo, H. Fu, Effects of Nb on microstructure and mechanical properties of Ti42Al2.6C alloys, Adv. Eng. Mater. 20 (2018) 1701112. doi:10.1002/adem.201701112

[17] M. W. Barsoum, M. Radovic, Elastic and mechanical properties of the MAX phases, Annu. Rev. Mater. Res. 41 (2011) 195–227. doi:10.1146/annurev-matsci-062910-100448.

[18] J. Lapin, A. Klimová, Vacuum induction melting and casting of TiAl-based matrix in-situ composites reinforced by carbide particles using graphite crucibles and moulds, Vacuum 169 (2019) 108930. doi:10.1016/j.vacuum.2019.108930

[19] J. Lapin, K. Kamyshnykova, Processing, microstructure and mechanical properties of in-situ Ti_3Al+TiAl matrix composite reinforced with Ti_2AlC particles prepared by centrifugal casting, Intermetallics 98 (2018) 34–44. doi:10.1016/j.intermet.2018.04.012

[20] O. Duygulu, High-resolution transmission electron microscopy investigation of in situ TiC/Al composites, Kovove Mater. 56 (2018) 265–275. doi:10.4149/km_2018_4_265

[21] A. Klimová, J. Lapin, T. Pelachová, Characterization of TiAl based alloys with various content of carbon, IOP Conf. Ser. Mater. Sci. Eng. 179 (2017) 012038. doi:10.1088/1757-899X/179/1/012038

[22] A. Klimová, J. Lapin, Effects of C and N additions on primary MAX phase particles in intermetallic Ti-Al-Nb-Mo matrix in-situ composites prepared by vacuum induction melting, Kovove Mater. 57 (2019) 1–7. doi:10.4149/km_2019_3_151

[23] A. Klimová, J. Lapin, Effect of Al content on microstructure of Ti-Al-Nb-C-Mo composites reinforced with carbide particles, Kovove Mater. 57 (2019) 377–387. doi:10.4149/km_2019_6_377

[24] A. Klimová, J. Lapin, Influence of Al content on morphology and properties of primary $(Ti,Nb)_2AlC$ particles in cast Ti-Al-Nb-Mo matrix in-situ composites, Proceedings of METAL 2019, 28th International Conference on Metallurgy and Materials (2019), pp. 6–11. ISBN 978-808729492-5

[25] Z. Wei, H. Wang, Y. Jin, H. Zhang, S. Zeng, Microstructures and mechanical properties of as-cast TiAl alloys with higher C additions, J. Mater. Sci. 37 (2002) 1809–1812. doi:10.1023/A:1014954024848

[26] J. Lapin, M. Štamborská, K. Kamyshnykova, T. Pelachová, A. Klimová, O. Bajana, Room temperature mechanical behaviour of cast in-situ TiAl matrix composite reinforced with carbide particles, Intermetallics 67 (2019) 158–165. doi:10.1016/j.intermet.2018.11.007

[27] W. Hua, X. Wu, D. Shen, H. Lu, M. Polak, Nanohardness and elastic modulus at the interface of TiC_x/Ni_3Al composites determined by the nanoindentation technique, Appl. Surf. Sci. 189 (2002) 72–77. doi:10.1016/S0169-4332(01)01050-9

[28] V. I. Ivashchenko, P. E. A. Turchi, A. Gonis, L. A. Ivashchenko, P. L. Skrynskii, Electronic origin of elastic properties of titanium carbonitride alloys, Metall. Mater. Trans. A 37 (2006) 3391–3396. doi:10.1007/s11661-006-1031-9

[29] Q. Yang, W. Lengauer, T. Koch, M. Scheerer, I. Smid, Hardness and elastic properties of Ti(C_xN_{1-x}), Zr(C_xN_{1-x}) and Hf(C_xN_{1-x}), J. Alloys Compd. 309 (2000) L5–L9. doi:10.1016/S0925-8388(00)01057-4.

[30] V. T. Witusiewicz, B. Hallstedt, A. A. Bondar, U. Hecht, S. V. Sleptsov, T. Y. Velikanova, Thermodynamic description of the Al-C-Ti system, J. Alloys Compd. 623 (2015) 480–496. doi:10.1016/j.jallcom.2014.10.119

[31] J. Yang, B. Cao, Y. Wu, Z. Gao, R. Hu, Continuous cooling transformation (CCT) behavior of a high Nb-containing TiAl alloy, Materialia 5 (2019) 100169. doi:10.1016/j.mtla.2018.11.018